PCCP

PAPER

View Article Online
View Journal | View Issue

Cite this: *Phys. Chem. Chem. Phys.*, 2014, **16**, 9580

Correlated fluorine diffusion and ionic conduction in the nanocrystalline F$^-$ solid electrolyte $Ba_{0.6}La_{0.4}F_{2.4}$—^{19}F $T_{1(\rho)}$ NMR relaxation *vs.* conductivity measurements

F. Preishuber-Pflügl,*[ab] P. Bottke,[a] V. Pregartner,[a] B. Bitschnau[c] and M. Wilkening*[ab]

Received 28th January 2014,
Accepted 26th March 2014

DOI: 10.1039/c4cp00422a

www.rsc.org/pccp

Chemical reactions induced by mechanical treatment may give access to new compounds whose properties are governed by chemical metastability, defects introduced and the size effects present. Their interplay may lead to nanocrystalline ceramics with enhanced transport properties being useful to act as solid electrolytes. Here, the introduction of large amounts of La into the cubic structure of BaF_2 served as such an example. The ion transport properties in terms of dc-conductivity values of the F$^-$ anion conductor $Ba_{1-x}La_xF_{2+x}$ (here with $x = 0.4$) considerably exceed those of pure, nanocrystalline BaF_2. So far, there is only little knowledge about activation energies and jump rates of the elementary hopping processes. Here, we took advantage of both impedance spectroscopy and ^{19}F NMR relaxometry to get to the bottom of ion jump diffusion proceeding on short-range and long-range length scales in $Ba_{0.6}La_{0.4}F_{2.4}$. While macroscopic transport is governed by an activation energy of 0.55 to 0.59 eV, the elementary steps of hopping seen by NMR are characterised by much smaller activation energies. Fortunately, we were able to deduce an F$^-$ self-diffusion coefficient by the application of spin-locking NMR relaxometry.

I. Introduction

Studying ion dynamics in solids is one of the most vital topics in modern solid-state chemistry.[1–3] The development of advanced sensors or energy storage systems requires careful examining of the correlation of ion transport over long distances and local ion hopping between neighbouring sites within a rigid lattice structure. Such studies are directly linked with the development of advanced solid electrolytes,[1–5] urgently needed for future all-solid-state rechargeable batteries.

In particular, highly conducting and electrochemically stable fluorides[5–9] are necessary components to bring all-solid-state fluorine-ion batteries[8] alive. Regarding particular applications they might serve as alternatives to those relying on lithium[2] and sodium[4] as ionic charge carriers. Quite recently, solid solutions of nanocrystalline fluorite-type $Ba_{1-x}La_xF_{2+x}$ prepared by high-energy ball milling have been introduced as a promising solid F$^-$ electrolyte.[9] First measurements of its electrochemical stability[10] encouraged us to study F dynamics in detail. As presented by Fichtner and co-workers,[9] ionic transport properties of a series of mechanochemically synthesized nanocrystalline samples with x ranging from $x = 0$ to $x = 0.55$ have been studied by impedance spectroscopy recently, and the data have been analysed with respect to macroscopic ion transport. Overall conductivity is anticipated to be fully governed by F anions, *i.e.*, the transference number is assumed to be close to one and, thus, no electronic contributions play a role practically. The highest ion conductivity was found for samples with $x = 0.3$ and $x = 0.4$.[9]

In the present study, we take advantage of ^{19}F nuclear magnetic resonance (NMR) relaxation measurements,[11,12] carried out under static conditions, to collect information on the elementary steps of ion hopping in structurally disordered $Ba_{0.6}La_{0.4}F_{2.4}$. NMR can be a powerful tool and has extensive applications in the field of fast (nanocrystalline) ion conductors, in particular.[13–22] It is worth noting that nanocrystalline $Ba_{1-x}La_xF_{2+x}$ is not stable in its nanostructured form at high temperatures; this restricts the temperature range, and thus also the number of available methods to probe diffusion parameters from an atomic scale point of view. NMR, however, offers quite a large set of techniques that are sensitive to both slow and fast (translational) ion dynamics. Here, with the use of SLR measurements, carried out in both (i) the rotating frame and (ii) the laboratory frame of reference,[11,23,24] F dynamics with jump rates ranging from the kHz to the MHz range can be probed. Their combination gives access to a quite large dynamic window.[25] Spin–spin relaxation

---

[a] Institute for Chemistry and Technology of Materials, and Christian Doppler Laboratory for Lithium Batteries, Graz University of Technology, Stremayrgasse 9, 8010 Graz, Austria. E-mail: preishuber-pfluegl@tugraz.at

[b] DFG Priority Program (SPP) 1415, Graz University of Technology, Stremayrgasse 9, 8010 Graz, Austria. E-mail: wilkening@tugraz.at

[c] Institute of Physical and Theoretical Chemistry, Graz University of Technology, Stremayrgasse 9, 8010 Graz, Austria

measurements[20] and line shape studies,[26] which do probe even slower F motions, complement the set of time-domain resonance techniques applied.

Considering fast ion conductors with a large number fraction of highly mobile ions, correlation effects[27–30] are expected to influence the movement of the charge carriers. Besides the possibility of quantifying F anion dynamics, as has been excellently presented by Chadwick and Strange,[31] NMR is also highly useful in distinguishing correlated from independent hopping.[18,26,32–35] In conjunction with conductivity spectroscopy,[28,36,37] complementary information of translational ion dynamics can be collected. Therefore, the present investigation is also aimed at contributing to the question[32,33,38] how results from various time domain NMR methods, *viz.* F migration activation energies and jump rates compare with those obtained from ac impedance spectroscopy, *i.e.*, probed on different length- and time scales. For this reason, impedance data have also been recorded over the whole temperature range covered by NMR, *i.e.*, including also temperatures well below ambient. In particular, the study presents impedance data recorded at frequencies as high as 3 GHz.

One major advantage of NMR is that it can often provide a direct estimate of the F^- jump rate[25,32] provided diffusion-induced contributions can be well separated from those being largely affected by so-called background relaxation. In the present case, with the spin-lock NMR technique, see, *e.g.*, ref. 39, it was indeed possible to record a diffusion-induced rate peak from which the self-diffusion coefficient D could be deduced. Our estimation uses the relaxation model of Bloembergen, Purcell and Pound[40] which was developed for three-dimensional (isotropic) motions of spin-1/2 nuclei moving in an uncorrelated manner. Finally, the NMR self-diffusion coefficient can be compared with solid-state diffusion coefficients extracted *via* the Nernst–Einstein equation from dc conductivity data.

II. Experiment

The $Ba_{1-x}La_xF_{2+x}$ sample with x = 0.4 has been prepared by high-energy ball milling[41–46] making use of a planetary mill (Fritsch, Pulverisette 7). The starting materials, powders of BaF_2 and LaF_3 with μm-sized crystallites, were purchased with high purity (99.99%) from Alfa Aesar and Sigma Aldrich, respectively. To synthesize several g of $Ba_{0.6}La_{0.4}F_{2.4}$, the binary fluorides were mixed under an Ar atmosphere according to the stoichiometric ratio needed. We used a beaker made of ZrO_2 (Fritsch) or tungsten carbide (Fritsch) equipped with 180 or 140 balls (5 mm in diameter) of the same material to treat the mixtures at 600 rpm under dry conditions. The ball-to-powder ratio was 17 : 1. We carefully avoided any contact with moisture; thus, the beakers were airtight filled with BaF_2:LaF_3 in a glove box with dry Ar atmosphere. Later on, *i.e.*, after milling periods ranging from 6 h to 10 h, they were also opened in the glove box.

Structural analysis of the prepared nanocrystalline powders was carried out using X-ray powder diffraction (XRPD) and magic angle spinning (MAS) NMR spectroscopy. The powder diffraction patterns, shown in Fig. 1, were recorded on a Bruker D8 Advance diffractometer with Bragg Brentano geometry using Cu K_α radiation (10–100° 2θ, step size 0.02° 2θ, step time 1 s). Rietveld refinement was carried out with X-PertHighScorePlus (PANalytical). ^{19}F MAS NMR experiments were recorded on a Bruker Avance III spectrometer operating at 470.5 MHz. We used a 2.5 mm-MAS probe (Bruker) with the ability to reach a spinning frequency of 30 kHz; spectra were recorded by non-selective excitation using a short pulse with a length of approximately 1.6 μs.

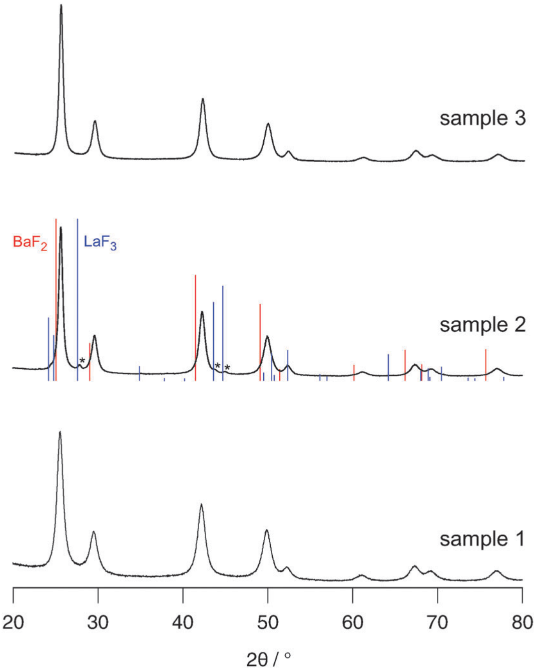

Fig. 1 X-ray powder diffractograms of the samples $Ba_{0.6}La_{0.4}F_{2.4}$ prepared for this study. For the synthesis of sample 1, a tungsten carbide vial set was used and the milling time was 6 h. Sample 2 was prepared with a ZrO_2 vial set and the mixture was treated for 6 h. Reflexes of residual LaF_3 are marked by asterisks. Sample 3 was also prepared using a ZrO_2 vial, but the milling time was increased to 10 h. As in the case of sample 1, no residual BaF_2 and LaF_3 are left.

To prepare dense pellets for impedance measurements the powder samples were cold-pressed by applying an uniaxial pressure of 0.13 GPa. Our press sets allow the fabrication of pellets with, *e.g.*, diameters of 5 mm, 8 mm and 10 mm (sample 3, see below). Pt electrodes (*ca.* 100 nm in thickness) were applied using a sputter coater (Leica). The thicknesses of the pellet pressed were measured with appropriate gauges. The impedance measurements were carried out using a Novocontrol Concept 80 broadband analyser (Alpha-AN, Novocontrol) being connected to a BDS 1200 cell in combination with an active ZGS cell interface (Novocontrol) allowing temperature-variable 2-electrode (dielectric) measurements. The temperature is automatically controlled by means of a QUATRO cryosystem (Novocontrol) making use of a heating element which builds up a specified pressure in a liquid nitrogen dewar in order to create a highly constant N_2 gas flow. After being heated by a gas jet, the freshly evaporated N_2 flows directly through the sample cell that is mounted in a cryostat. This setup allows very stable system operation with an accuracy of ±0.01 °C. In summary, the whole setup is able to record the complex impedance ($\hat{Z}$) and the permittivity ($\hat{\varepsilon}$) at frequencies ranging from few μHz up to 20 MHz (110–570 K). For impedance measurements up to 3 GHz we used an Agilent E4991 A high-frequency analyser connected to a high frequency cell (Novocontrol).

For the NMR measurements the fluoride was sealed in glass ampoules, *ca.* 4 cm in length and 5 mm in diameter, to protect the nano-crystalline samples with their large surface area permanently from any influence of humidity. NMR lines and relaxation rates were measured using an Avance III spectrometer connected to a shimmed cryomagnet with nominal magnetic fields of 7 T. This field corresponds to a ^{19}F Larmor frequency of $\omega_0/2\pi$ = 282 MHz. We used a home-built (high-temperature) NMR probe capable of recording NMR signals under static, *i.e.*, non-rotating conditions up to temperatures as high as 550 K. The $\pi/2$ pulse length was approximately 1 μs at 200 W. A Eurotherm temperature controller in combination with a type *T* thermocouple was used to control and monitor the temperature in the probe's sample chamber.

^{19}F NMR spin-lattice relaxation (SLR) rates $1/T_1$ were acquired with the saturation recovery pulse sequence $10 \times \pi/2–t_d–\pi/2–$acquisition (acq.)[47,48] The pulse sequence works as follows: an initial pulse train, consisting of ten $\pi/2$ pulses separated by 40 μs, was used to destroy any longitudinal magnetization M_z prior to recording its temperature-dependent recovery as a function of the delay time t_d. Rotating-frame ^{19}F NMR SLRϱ rates $1/T_{1\varrho}$ were recorded with the spin-lock technique, $\pi/2\ p(t_{\mathrm{lock}})$–acq.[39,47,49–53] With our probe we were able to make use of a locking frequency ω_1 of approximately 62.5 kHz. The corresponding locking pulse t_{lock} was varied from 40 μs to 400 ms. Note that the recycle delay for the SLRϱ experiments was set to at least $5 \times T_1$ in order to guarantee full longitudinal relaxation between each scan. $1/T_{1(2)}$ and $1/T_{1\varrho}$ rates were obtained by parameterizing the magnetic transients $M_z(t_d)$ and $M_\varrho(t_{\mathrm{lock}})$, respectively, by stretched exponentials: $M_z(t_d) \propto 1 - \exp(-(t/T_1)^\gamma)$ and $M_\varrho(t_{\mathrm{lock}}) \propto \exp(-(t_{\mathrm{lock}}/T_{1\varrho})^{\gamma_\varrho})$, respectively (*cf.* Fig. 2).

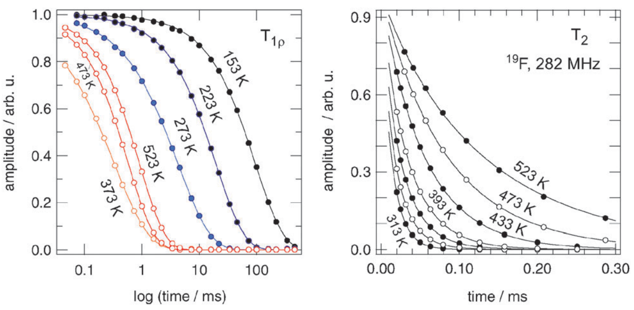

Fig. 2 Left: ^{19}F NMR transversal decay of the spin-locked magnetization recorded at the various temperatures indicated. The locking frequency was 62.5 kHz. Note the logarithmic scale of the *x*-axis. Solid line represent fits according to stretched exponentials yielding $T_{1\rho}^{-1}$ and $\gamma_{1\rho}$. Right: ^{19}F NMR spin–spin relaxation transients. From the fits (stretched exponentials, solid lines) the rates T_2^{-1} and stretching factors γ_2 shown in the upper part of the Arrhenius plot of Fig. 3 can be obtained. The corresponding T_1-transients do almost follow an exponential time behaviour.

In addition, temperature-variable ^{19}F NMR spin–spin relaxation (SSR) rates $1/T_2$ were recorded by taking advantage of a (two-pulse) solid-echo pulse sequence:[47] $\pi/2–t_{\mathrm{echo}}–\pi/2$–acq. t_{echo} denotes the variable interpulse delay. The transients obtained were fitted with stretched exponentials. Static ^{19}F NMR spectra were either obtained after Fourier transformation (FT) of the free induction decay, which were recorded by non-selective irradiation with a single $\pi/2$ pulse, or by FT of the solid echo beginning from the top of the signal.

III. Results and discussion

A. Characterization by X-ray diffraction

Phase purity of the mechanochemical preparation of nanocrystalline $Ba_{0.6}La_{0.4}F_{2.4}$ was checked by powder X-ray diffraction carried out at room temperature and in air atmosphere. In Fig. 1 the diffractograms of several samples, which have been differently prepared, are shown. While sample 1, which was prepared in a tungsten carbide (WC) vial (t_{mill} = 6 h), does not reveal any binary fluorides left, sample 2, which was synthesized under slightly different milling conditions (ZrO_2 vial, t_{mill} = 6 h), shows residual LaF_3. According to Rietveld refinement, phase pure $Ba_{0.6}La_{0.4}F_{2.4}$ is formed in the ZrO_2 beaker, when the milling time t_{mill} to prepare the ternary fluoride is increased from 6 h to 10 h (sample 3). The vertical bars in Fig. 1 represent positions and intensities of the reflexes of the two starting materials. The systematic shift of the diffraction angle 2θ towards larger values points to lattice contraction due to the incorporation of the smaller La ions into the fluorite structure of BaF_2.[9]

From the broadening of the reflexes we estimated an average crystallite size of approximately 10 nm (Scherrer equation). Such a value is typically found for mechanosynthesized ceramics treated in high-energy ball mills. The X-ray powder patterns show a low and straight-line background and, therefore, no indications for notable amounts of the amorphous material present. Sample 1 has been used for ^{19}F NMR and impedance measurements up to 20 MHz. From sample 3 a larger pellet with a diameter of 10 mm was pressed for high-frequency impedance measurements carried out up to 3 GHz.

B. NMR measurements

Compared to the recently published study of Rongeat *et al.*,[9] which mainly focusses on the investigation of F ion transport in $Ba_{1-x}La_xF_{2+x}$ by impedance spectroscopy, we emphasized on static ^{19}F NMR relaxometry to point out the differences between short- and long-range F diffusivity. To that end, the present study centres upon a single mechanosynthesized sample with x = 0.4 which is the composition leading to the highest conductivity observed.[9] In the Arrhenius plot of Fig. 3(a) an overview of the NMR relaxation rates measured is shown. The figure presents the temperature-dependent relaxation rates $1/T_1$, $1/T_{1\rho}$, and $1/T_2$ together with the stretching exponents γ_i (i = 1, 1ρ, 2) obtained by parameterizing the underlying magnetization transients (see Fig. 2) with appropriate fitting

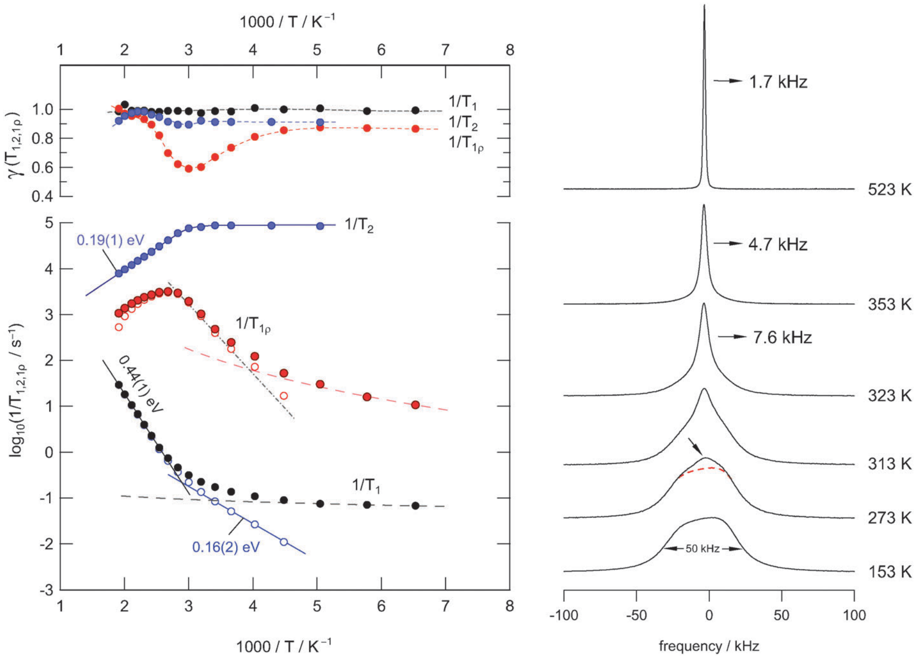

Fig. 3 Left: temperature dependence of the ^{19}F NMR relaxation rates of nanocrystalline Ba$_{0.6}$La$_{0.4}$F$_{2.4}$ (sample 1) prepared by mechanosynthesis at ambient temperature. The Larmor frequency was 282 MHz. The upper graph shows the dependence of the stretching exponents γ on T. Right: ^{19}F NMR line shapes recorded under static conditions at the temperatures T indicated.

functions;[34] in our case stretched exponentials were used (see above). For comparison, on the right-hand side of Fig. 3 a couple of temperature-variable ^{19}F NMR spectra of mechanosynthesized Ba$_{0.6}$La$_{0.4}$F$_{2.4}$ are shown.

Starting the discussion with the ^{19}F NMR spectra, which were recorded under non-rotating conditions, it is evident that at the lowest temperature, being accessible with the probe used here, the overall NMR signal is composed of several components. Owing to both structural disorder and cation mixing introduced during milling, the shape of the low-T spectrum likely reveals a superposition of many NMR intensities that reflect magnetically different F species. These species result from a broad distribution of locally distinct environments. For comparison, it is known for pure nanocrystalline BaF$_2$, even if severely treated in shaker or planetary mills, that the corresponding ^{19}F NMR signal is much less broadened than it is found in the present case.[43]

Here, the overall shape of the NMR spectra recorded at low T results from the mixing effect of Ba and La ions; this alters the ^{19}F chemical shifts. Similarly, this has also been reported by Fichtner and co-workers using magic angle spinning (MAS) ^{19}F NMR on samples with varying La-content.[9] For comparison, in cation-mixed mechanosynthesized (Ba,Ca)F$_2$, as well as in mixed fluorides with Sr and Ca ions, the individual F environments could be well resolved due to relatively sharp resonance lines and the application of high-speed MAS NMR.[44]

As it becomes obvious from Fig. 3(b), with increasing temperature a narrowed NMR line emerges which is due to both averaging of dipole–dipole[26] and local chemical shift interactions of the various magnetically inequivalent F ions. At sufficiently high temperatures the mean exchange rate becomes much faster than the spectral width of the NMR line. This slows down spin–spin relaxation and leads to a single NMR line being fully narrowed by motional averaging; see the spectrum recorded at 523 K, which is the upper temperature we used for our study. Compared to the initial situation, the line width (full width at half maximum) has been decreased from *ca.* 50 kHz down to 1.7 kHz; in the regime of *extreme averaging* it is mainly governed by inhomogeneities of the external magnetic field. From motional averaging it is evident that the jump rate τ^{-1} (523 K) is much larger than 50 kHz × 2π, *i.e.*, the rate should be in the order of 10^5 s^{-1} to 10^6 s^{-1}.

In Fig. 4 selected ^{19}F NMR spectra are shown which were deconvoluted by using a Gaussian and a Lorentzian line (see the solid and dashed lines of the spectra recorded at 323 K and 353 K, respectively). At higher temperatures, *i.e.*, in the regime of full averaging, *viz.* at 523 K, the NMR line can be best represented by a single Voigt profile. In general, such heterogeneous motional narrowing can be linked with a distribution of F$^-$ jump rates. Cation mixing[44] and local structural disorder in nanocrystalline Ba$_{0.6}$La$_{0.4}$F$_{2.4}$ prepared by mechanical treatment supports this idea. Thus, the rate estimated above should be regarded as a mean value.

According to a mean jump rate in the order of or even larger than 10^4 s^{-1}, the ^{19}F NMR spin–spin and spin–lattice relaxation rates are expected to be greatly, if not solely, influenced by F self-diffusion. F dynamics lead to fluctuations of the local dipolar fields and induce longitudinal magnetization recovery as well as affect transversal NMR relaxation. Starting the analysis with the laboratory-frame SLR rates, we observe a weaker-than-activated temperature dependence below 225 K (see Fig. 3(a)). In this low-T regime, which is characterised by $\omega_0\tau_c \lll 1$ where τ_c is

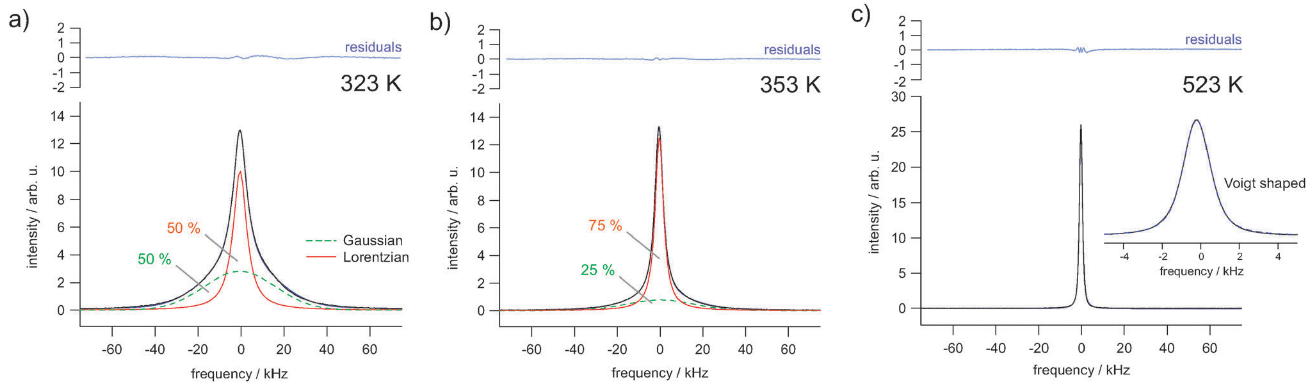

Fig. 4 Selected ^{19}F NMR lines to highlight the motional averaging of dipole–dipole interactions and coalescence as well. While a combination of a Gaussian and a Lorentzian is appropriate to represent the lines at moderate temperatures, the final shape in the regime of extreme narrowing resembles that of a Voigt function. The values in percentage terms indicate the area fractions of the two different components.

the motional correlation time, T_1^{-1} is mainly driven by non-diffusive relaxation sources such as lattice vibrations and coupling of the spins with paramagnetic impurities. With increasing temperature, however, the rate T_1^{-1} increases; at $T > 370$ K it has already reached the low-T flank ($\omega_0\tau_c \ll 1$) of the diffusion-induced rate peak, which is expected to show up at higher T. It should be noted that temperatures well above 550 K are not accessible with the NMR setup available in our laboratory. Moreover, the onset of grain growth may represent a natural limit to investigate F diffusion parameters in nanocrystalline (metastable) fluorides.

In order to carefully separate non-diffusive background relaxation from purely diffusion-induced contributions, we parameterized the low-T rates with an appropriate power law $T_1 \propto T^{\beta}$ and extrapolated the rates obtained to higher temperatures (see the dashed line in Fig. 3(a)). Subsequent subtraction from the overall rates measured resulted in background-corrected SLR rates which are represented in Fig. 3 by unfilled symbols. As a result, we observe a stepwise increase in the diffusion-induced T_1^{-1} rates: starting from low T an activation energy of $E_a'' = 0.16$ eV can be deduced, while an Arrhenius fit of the flank showing up at higher temperatures yields $E_{a,low} = 0.44$ eV.

The first value nicely agrees with the one obtained from spin–spin-relaxation measurements which are also shown in Fig. 3. In the limit $T \rightarrow 0$ K, which is the rigid lattice, T_2^{-1} is approximately given by 10^5 s$^{-1} \equiv T_{20}^{-1}$. The rate T_2^{-1} starts to deviate from T_{20}^{-1} at 330 K and then follows an Arrhenius law characterised by an activation energy of only $E_a' = 0.19$ eV. According to the simple behaviour expected from the relaxation model of Bloembergen, Purcell and Pound (BPP), which had been introduced for 3D (isotropic) uncorrelated motion,[40] one would expect the T_2^{-1} flank to coincide with the high-T flank ($\omega_0\tau_c \gg 1$) of the T_1^{-1} rate peak leading to $E_a' = E_{a,high}$ with $E_{a,high}$ being the activation energy in the regime $\omega_0\tau_c \gg 1$. It should be noted that $E_{a,high}$ cannot be determined *via* T_1^{-1} measurements in the present case because of temperature restrictions and limitations in our experimental setup (see above).

The various models developed for correlated motions do predict asymmetric NMR rate peaks.[14,17,30] Indeed, such shapes are observed in general; the corresponding peaks are characterised by $E_{a,low}$ being smaller than $E_{a,high}$ and $E_a' = E_{a,high}$, respectively. $E_{a,high}$ is often compared with the corresponding value from dc conductivity measurements (see Fig. 5 and the following section).[32] In our case, however, these general characteristics for correlated 3D jump diffusion seem to be not fulfilled and an anomaly is observed as will be outlined in detail in the following.

To shed further light on this situation, we recorded ^{19}F $T_{1\rho}$ NMR SLR rates in the rotating frame of reference at locking frequencies much smaller than the Larmor frequency used for our T_1 measurements. Compared to NMR relaxometry in the lab frame, $T_{1\rho}^{-1}$ is *per se* sensitive to F motions taking place on a longer length (and time) scale.[17] As expected, we were able to partly reach the high-T flank of the corresponding $T_{1\rho}^{-1}(1/T)$ peak; compared to $T_1^{-1}(1/T)$ it is shifted towards lower T. The peak itself spans a rather broad T range; even after appropriate background correction, as it was done for T_1, the high-T flank cannot be clearly separated. The broadened peak might be the result of superimposing rate peaks reflecting the distribution of migration processes in the disordered $Ba_{0.6}La_{0.4}F_{2.4}$ phase. Irrespective of its overall shape, the activation energy in the limit $\omega_1\tau_c \ll 1$ lies in the range 0.25–0.35 eV. The resulting value depends on the quality of the correction procedure applied, *i.e.*, the β chosen, and the number of data points taking into account for the Arrhenius fit. Most importantly, these values are even smaller than $E_{a,low}$ deduced from $T_1^{-1}(1/T)$ in the limit $\omega_0\tau_c \ll 1$. This points to a second anomaly observed *via* NMR relaxation. Frequency-dependent conductivity measurements might help understand the complex results found by NMR relaxometry.

C. Impedance and dielectric measurements

Quite recently, impedance spectra, that is the real part σ' of the complex conductivity ($\hat{\sigma}$) plotted *vs.* frequency ν, have been reported by Fichtner and co-workers;[9] conductivity data were discussed in terms of contributions from bulk and grain boundaries of mechanosynthesized $Ba_{1-x}La_xF_{2+x}$. To compare our results from NMR, recorded at lower temperatures and resonance frequencies in the kHz and MHz range, the samples have been investigated at temperatures down to 173 K and at

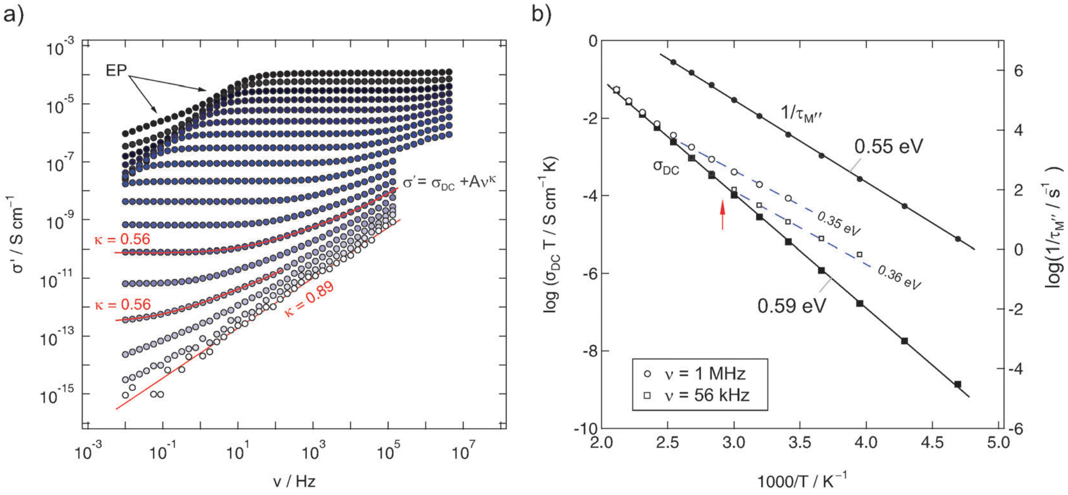

Fig. 5 (a) impedance isotherms of mechanosynthesized $Ba_{0.6}La_{0.4}F_{2.4}$ (sample 1) recorded at temperatures ranging from 133 K up to 473 K. (b) Arrhenius plot of $\sigma_{DC}T$; for comparison, the temperature dependencies of $\sigma'T$, read out at frequencies ν = 1 MHz and 56 kHz, respectively, are also shown. Moreover, $\tau_M{}^{-1}$, that is the relaxation rate being determined from modulus spectra $M''(\nu)$, is also presented.

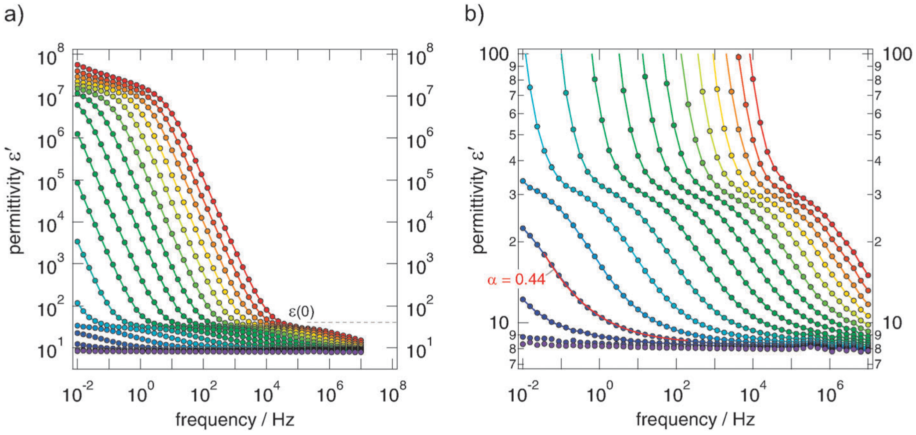

Fig. 6 (a) Real part of the complex permittivity ε' of nanocrystalline $Ba_{0.6}La_{0.4}F_{2.4}$ (sample 1) as a function of frequency ν. (b) Magnification of the spectra shown left in order to estimate $\varepsilon(0)$. The bulk process can be mirrored with a power law of the form $\varepsilon'(\nu) = \varepsilon(\infty) + A_\varepsilon \nu^{-p}$ with $p \neq f(t) \approx 0.44$.

frequencies as high as 3 GHz. In Fig. 5–7 selected conductivity as well as permittivity spectra are shown.

The isotherms (sample 1) shown in Fig. 5(a) reveal the typical characteristics of impedance spectra of structurally disordered materials usually showing a distribution of jump rates and activation energies. If not perturbed by electrode polarisation (EP) effects, dominating impedance response at high temperatures and low frequencies, the spectra are composed of a dc-plateau and a Jonscher-type dispersive region, which can be approximated with a power law according to $\sigma' = \sigma_{DC} = A_\sigma \nu^\kappa$. As has been shown by many previous studies on other ion conductors, the exponent κ takes values ranging from 0.5 to 0.8. In our case we found $\kappa = 0.56$ almost independent of T. $\kappa \neq f(T)$ means that the isotherms have the same shape and can be collapsed into a single so-called master curve after appropriate scaling has been carried out. This behaviour indicates that impedance spectroscopy, when carried out at different temperatures ($>$193 K) and frequencies with values as high as 1 MHz, is sensitive to the same motional process in $Ba_{0.6}La_{0.4}F_{2.4}$.

At the lowest temperatures, that is, at temperatures lower than 173 K, the dc-plateau has been mainly shifted towards lower frequencies and a $\nu^{0.89}$-dependence shows up. The increase of κ towards larger values might be related to the presence of strictly localized F motions governing the isotherms at sufficiently low T. κ being close to 1 would correspond to the (nearly) constant loss (NCL) phenomenon which is frequently related to such caged dynamics, see, *e.g.*, ref. 28 for a brief overview on this topic.

In order to quantify thermal activation of long-range F transport, DC conductivity values ($\sigma_{DC}T$) have been plotted in Fig. 5(b) *vs.* 1000/T. The solid line represents a linear fit and yields an activation energy $E_{a,dc}$ of 0.59 eV. This result is in very good agreement with the value found by Rongeat *et al.*[9] (0.58 eV) and with those reported for F^- ion transport in single crystals.[54–56] Moreover, it is comparable with the activation energy when electrical relaxation times $\tau_{M'}$ are analysed, which

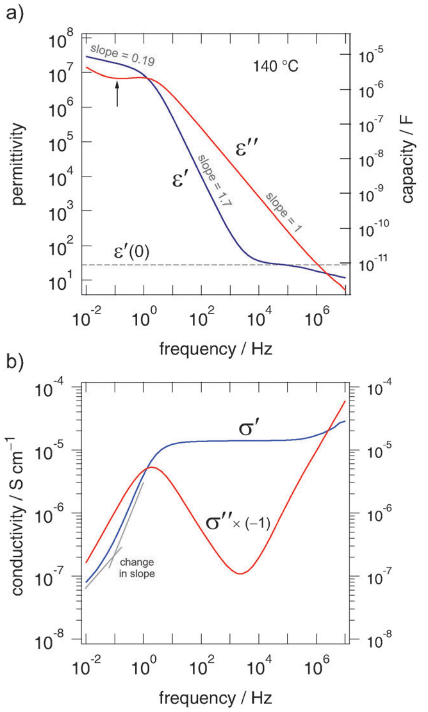

Fig. 7 (a) The frequency dependence of ε' and ε'' recorded at 413 K. (b) Frequency dependence of σ' and $(-1)\cdot\sigma''$ recorded at 413 K. According to the Kramers–Kronig relation and $\hat{\sigma}(\omega) = i\omega\varepsilon_0\hat{\varepsilon}(\omega)$ (here, we have $\omega/2\pi = \nu$, $i^2 = -1$ and ε_0 being the permeability under vacuum) the plateau $\sigma' \propto A_\sigma\nu^0$ corresponds to $\varepsilon'' \propto A_\varepsilon\nu^{-1}$. The local minimum of ε'' (see arrow) is expressed as a change in slope in the EP region of σ', see also Fig. 5. The slopes given for ε' indicate electrode polarisation.

can be deduced from modulus peaks $M''(\nu)$. These are less sensitive to an electrical response determined by large capacities such as the response from grain boundaries. Hence, we may assume that σ_{DC} mainly reflects the bulk response and that grain boundaries seem to play a less prominent role in blocking long-range transport. As has been pointed out by Rongeat *et al.*,[9] the activation energy obtained from $\sigma_{DC}T$ *vs.* $1/T$ mainly reflects the migration enthalpy rather than contributions from forming F vacancies. The authors already have pointed out that activation energies ranging from 0.5 to 0.6 eV would correspond to those being characteristic for vacancy migration in microcrystalline BaF_2 (and its single crystals).[31,57] In a structurally disordered material, particularly when prepared by mechanical treatment, also other point defects such as F interstitials have to be considered – especially in the case of La-doped BaF_2. In such a case, specifying a primary point defect, if there is any, is very difficult. Most likely, the situation has to be described by a complex interplay of different kinds of defects, including not only point defects.

To judge which capacities and permittivities are associated with the impedance spectra and dc-plateaus obtained, we plotted ε' as a function of ν (see Fig. 6). Starting with $\varepsilon'(\infty) \approx 8$ at low temperatures and high frequencies, at intermediate temperatures a plateau is reached indicating that $\varepsilon'(0)$ is approximately 35 (see the magnification in Fig. 6(b)). The corresponding capacity takes a value of approximately 9 pF (Fig. 7). In our opinion these values corroborate the anticipation that σ_{DC} is predominantly determined by the bulk response. The further increase of ε' observed is due to polarisation effects of the ion blocking electrodes applied. In Fig. 7 the real and imaginary parts of $\hat{\sigma}$ and $\hat{\varepsilon}$ are compared. The curves reveal the well-known features of impedance spectroscopy and show an almost 'ideal' frequency dependence that is expected for a non-Debye impedance response. This is also expressed as follows. If ε' is given by $\varepsilon'(\nu) = \varepsilon'(\infty) + A_\varepsilon\nu^{-p}$ an AC storage-to-loss ratio of one is obtained if $p + \kappa = 1$. Indeed, our data fulfill this relation; we have $\kappa = 0.56$ and $p = 0.44$ (see Fig. 6(b)).

At this stage let us start comparing the results from impedance spectroscopy with those from NMR relaxometry. Even if $E_{a,dc}$ represents bulk properties, it cannot be expected to fully match $E_{a,low}$ from NMR. The two methods are sensitive to anion motions taking place on quite different time scales and they have to be described by distinct motional correlation functions. If at all, $E_{a,dc}$ is expected to coincide with $E_{a,high}$;[17] the latter is *per se* sensitive to long-range ion motion at least. In contrast to $E_{a,high}$, the low-T flank of a given T_1^{-1} rate peak is affected by correlation effects such as structural disorder and Coulomb interactions.[27,29] Such interactions lead to the aforementioned asymmetry of an NMR rate peak.

If we, however, readout conductivities at higher frequencies instead of determining dc-values at $\nu \to 0$, lower activation energies should result.[26,32] Indeed, this is the case when the Arrhenius plot of Fig. 5 is considered. The unfilled symbols represent $\sigma'T$ measured at 56 kHz and 1 MHz. Although, as expected, the values coincide with $\sigma_{DC}T$ at sufficiently high temperatures, the deviations at lower T hint to smaller activation energies being responsible for anion hopping if shorter length scales are regarded. Typically, $E_{a,ac} = 0.35$ eV is obtained here, that is, however, smaller than $E_{a,low}$ from ^{19}F NMR. Instead, good agreement has been found between $E_{a,low}$ and $E_{a,ac}$ in the case of nanocrystalline $LiTaO_3$ analysed in a similar manner. Such an agreement is proposed by the coupling concept introduced by Ngai[32] and has been documented for a number of ion dynamics in glassy systems, in particular.

Although $E_{a,ac}$, irrespective of being determined at 56 kHz or 1 MHz, might be interpreted as an activation energy that is comparable with that of the low-T flank of the $T_{1\rho}^{-1}$-peak, the discrepancy between $E_{a,ac} = 0.35$ eV and $E_{a,low} = 0.44$ eV is apparent. To answer the question whether this changes the frequency regime that is identical with the Larmor frequency of 282 MHz, we performed conductivity measurements up to the GHz range. In Fig. 8 some of the impedance data of sample 3 are shown. The conductivities recorded span a dynamic range of eleven decades. The data points recorded in the GHz regime perfectly match those collected with the Alpha-analyser working up to 20 MHz. As a side note, the high-frequency data reveal a change in the slope of the isotherms recorded at low temperatures. This might be an indication of a high-frequency plateau increasingly affecting conductivity data.

At high temperatures, ac conductivities σ' determined at 282 MHz, which equates the NMR Larmor frequency, do also follow an Arrhenius law with an activation energy of 0.35 eV (see Fig. 8). Of course, at lower temperatures the influence of an

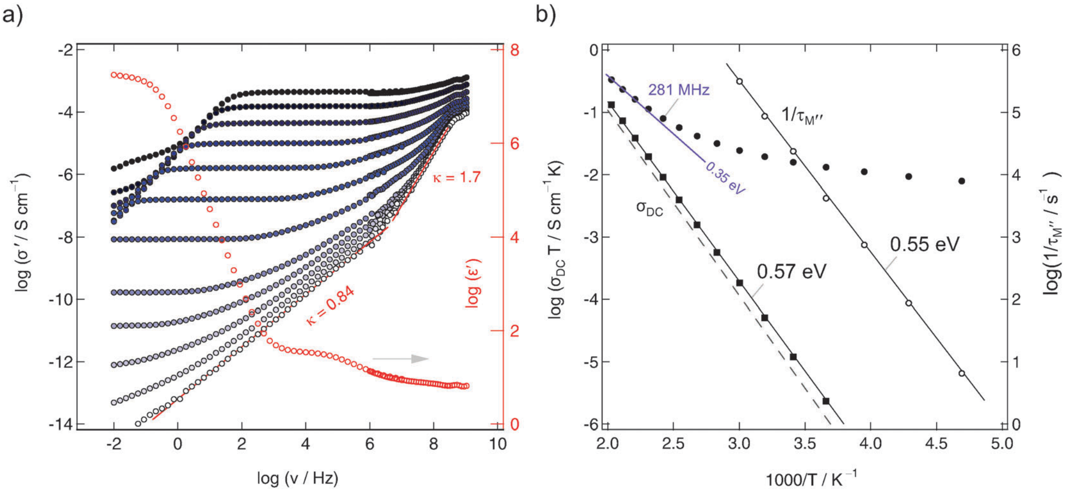

Fig. 8 (a) Full conductivity (and permittivity, 373 K) isotherms of nanocrystalline $Ba_{0.6}La_{0.4}F_{2.4}$ (sample 3) covering a frequency range of eleven decades. Temperatures range from 153 K to 513 K in steps of 20 K. (b) Corresponding Arrhenius plot showing the temperature behaviour of $\sigma_{DC}T$ of sample 3 (see above) and $\sigma'(\nu = 282\ \text{MHz})T$. Note that 282 MHz equates the ^{19}F NMR Larmor frequency. The lines show linear fits; the activation energies are indicated. For comparison, the dashed line represents $\sigma_{DC}T$ of sample 1, which has been prepared in a tungsten carbide vial.

NCL-type contribution increases and $\sigma'(T)$ reveals only a weak dependence on T. Let us identify the ac activation energy of 0.35 eV with that of short-range ion motion affected by correlated forward–backward jumps and $E_{a,dc}$ with that of long-range translational ion hopping. If we do so, the difference $E_{a,dc} - E_{a,ac} \approx 0.22$ eV could be interpreted in terms of the jump relaxation model as an activation energy needed for the surrounding lattice to relax towards a new equilibrium state accommodating the ion just jumped to a vacant site.[58]

Lastly, in order to compare the response of conductivity spectroscopy with that of NMR, within an extra experiment we recorded σ' (and ε') at a single frequency but varied the temperature. In Fig. 9 the real part of the complex resistivity, which is given by $\hat{\rho} = 1/\hat{\sigma}$ and related to the complex modulus according to $\hat{M} = 1/\hat{\varepsilon}$ *via* $\hat{\rho} = \hat{M}/(i\omega e_0)$, is plotted *vs.* the inverse temperature. ρ' passes through distinct maxima. If recorded at 60 kHz the peak shows up at $T \approx 335$ K; this result is in good agreement with the position of the corresponding $1/T_{1\rho}(1/T)$-peak, see Fig. 3. As expected, the $\rho'(1/T)$-peak shifts towards higher T with increasing frequency. The slope of the high temperature flank yields $E_{a,\rho} = 0.55$ eV ($\approx E_{a,dc}$) (see the solid line drawn).

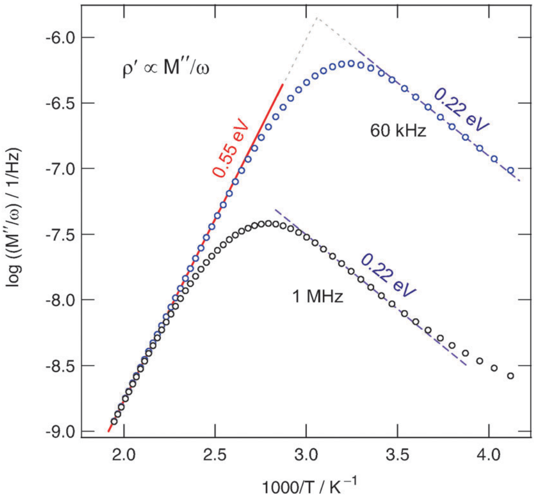

Fig. 9 Real part of the complex resistivity of nanocrystalline $Ba_{0.6}La_{0.4}F_{2.4}$ (sample 3) as a function of inverse temperature T. From the different flanks of asymmetric peaks obtained activation energies for long- and short-range motion can be deduced.

The pronounced asymmetry of the peaks is in agreement with that commonly found for glassy or at least structurally disordered ion conductors, see ref. 59, in particular. Important to note, the rather broad shape of the maximum resembles that of the $1/T_{1\rho}(1/T)$ peak. It is an indication of a broad distribution of different relaxation mechanisms present. Before we finally compare the various activation energies obtained, we will contrast the self-diffusion coefficient obtained from the $1/T_{1\rho}(1/T)$ peak with that which can be deduced from σ_{dc}. According to the NMR maximum conditions in the rotating frame of reference $\omega_1\tau \approx 0.5$, the jump rate is in the order of $7.85 \times 10^5\ \text{s}^{-1}$. With the Einstein–Smoluchowski equation $D_{sd} = \ell^2/(6\tau)$ for 3D diffusion[60] this translates into a self diffusion coefficient D_{sd} of $1.2 \times 10^{-14}\ \text{m}^2\ \text{s}^{-1}$ at 380 K if we assume a jump distance ℓ of approximately 3 Å. Reducing ℓ to 2 Å, D_{sd} decreases to $5.2 \times 10^{-15}\ \text{m}^2\ \text{s}^{-1}$.

However, the Nernst–Einstein equation relates σ_{dc} with a solid-state diffusion coefficient D'.[60] According to our conductivity values, diffusion coefficients of $D'(373\ \text{K}) \approx 3.0 \times 10^{-15}\ \text{m}^2\ \text{s}^{-1}$ and $D'(393\ \text{K}) \approx 7.6 \times 10^{-15}\ \text{m}^2\ \text{s}^{-1}$ are obtained. While D' is related to the tracer diffusion coefficient *via* $D_{tr} = H_R D'$ with the Haven ratio H_R; D_{sd} given by $D_{tr} = fD_{sd}$ and f denotes the correlation factor ranging from 0 to 1. Altogether this leads to $D_{sd} = (H_R/f)D'$. Assuming that the quotient H_R/f is in the order of unity, good agreement between σ_{dc} and the appearance of the $1/T_{1\rho}(1/T)$ rate peak is obtained. The high-temperature flank of the NMR peak is expected to be governed by an activation energy being similar to that found by dc conductivity measurements.

Table 1 Activation energies E_a from the various NMR and conductivity methods applied

Method	E_a (eV)	Type	T-range, frequency
T_1	0.16(2)	I	220–330 K, 116 MHz
T_2	0.19(1)	I	350–550 K, 116 MHz
ρ'	0.22(2)	I	Low-T flank of (M''/ω)-peaks
σ' ac	0.35(3)	II	250–500 K, 56 kHz–282 MHz
$T_{1\rho}$	0.25–0.35	II	250–330 K, 56 kHz
T_1	0.44(1)[a]	III	400–530 K, 116 MHz
$\tau_{M''}$	0.55(1)	IV	220–400 K, modulus peaks
ρ'	0.55(1)	IV	High-T flank of (M''/ω)-peaks
σ' dc	0.57(1)	IV	200–500 K (sample 3)
σ' dc	0.59(1)	IV	200–500 K (sample 1)

[a] Low-T flank of the $1/T_1(1/T)$-peak.

D. Final discussion and comparison of activation energies

To sum up, in Table 1, the activation energies probed by both impedance and NMR spectroscopy are listed. Disregarding fully NCL-type caged dynamics (see above), the different regimes of activation energies probed illustrate the transition from short-range motions (I and II) to long-range ion transport (IV).

The data clearly illustrate that the final result for the activation energy is determined by the method chosen and its sensitivity to a specific time and length scale. Only in structurally ordered and (macroscopic) homogeneous materials with a perfectly regular energy landscape one might expect a single value for the activation energy E_a.

While the activation energy of type I might point to localized dynamics, group II could be identified with the (mean) activation energy describing the elementary jump processes in nanocrystalline $Ba_{0.6}La_{0.4}F_{2.4}$. The relatively large value probed by T_1 NMR seems to reflect an anomaly coupled with the different jump mechanisms leading to long-range ion transport. It is worth noting that the latter result does not depend on the integration range of the underlying NMR free induction decays. This means that it does not play a role whether parts of the free induction decays or the whole integral over the transient signal is analysed in terms of a saturation recovery experiment to extract the T_1 rates. In all cases the same magnetization recovery curve is obtained which follows a pure exponential containing a single T_1^{-1} rate. Hence, from the point of view of SLR NMR the spin ensemble appears as a dynamically uniform system. Even if there are any microscopic spin regions acting differentially, fast spin-diffusion, *i.e.*, so-called spin flip-flop processes without mass transfer, results in a homogeneous ^{19}F NMR spin system characterised by a single spin temperature.

IV. Conclusions

Up to a certain concentration the mechanochemical introduction of La ions into BaF_2 leads to solid solutions of $Ba_{1-x}La_xF_{2+x}$ crystallizing with a fluorite-type structure.[9] Structural disorder and strain owing to the socialization of two cations with largely different radii, see also ref. 44, is anticipated to severely affect overall ion transport of F^-. The relatively high ion conductivity of $Ba_{1-x}La_xF_{2+x}$ with $x = 0.4$ at elevated temperatures makes the cation-mixed material a promising solid electrolyte in modern energy storage systems with F^- ions as charge carriers. Preliminary solid-state cyclovoltammetry measurements[10] encouragingly show a sufficiently good electrochemical stability over a relatively large potential window.

Here, we could show, by using both atomic-scale NMR relaxometry and (high-frequency) broadband impedance spectroscopy, that F^- ion transport in the ternary fluoride is governed by multiple hopping processes. Depending on the time scale the particular technique is sensitive to, we could distinguish between short-range and long-range translational dynamics. This manifests in a broad range of activation energies found spanning the range from localized hopping (0.16 eV) to macroscopic ion transport (0.55 eV). Interestingly, an anomaly is found when activation energies obtained from ac conductivity spectroscopy (0.35 eV) are compared with that deduced from diffusion-induced T_1^{-1} ^{19}F NMR performed at 282 MHz. This might be explained by the fact that the two methods, even if applied in the same frequency window, do probe different motional correlation functions. Structural heterogeneities, such as the formation of F^- clusters,[9,54,55,61] or size effects such as the influence of space charge zones[62,63] in materials with a large surface area might also be considered to discuss the results found. To this end, detailed structural information is needed to correlate them with the dynamic properties studied here.

Unfortunately, due to the heat sensitivity of the sample we could not probe the high-temperature flank of the corresponding ^{19}F NMR peak in the rotating frame of reference. Fortunately, *via* the shallow maximum detected at approximately 380 K the F self-diffusion coefficient D_{sd} could be determined. A value of 7.85×10^5 s^{-1} is in line with that which can be estimated from dc conductivity results. This is consistent with the agreement between activation energies from ac conductivity and the low-T flank of the $T_{1\rho}^{-1}$ NMR peak.

Author contributions

The authors were equally involved in experimental work, data analysis and project planning. All authors have given approval to the final version of the manuscript.

Acknowledgements

We thank our colleagues at the TU Graz and the University of Hannover, especially A. Düvel, for valuable discussions concerning sample preparation and characterisation. Financial support by the Deutsche Forschungsgemeinschaft (DFG), SPP 1415, the Austrian Federal Ministry of Economy, Family and Youth, and the Austrian National Foundation for Research, Technology and Development is greatly appreciated. Furthermore, we thank the DFG for access to the NMR and impedance spectrometers of the DFG Research Unit 1277, grant no. WI3600/2-1 and 4-1.

References

1 K. Funke, *Sci. Technol. Adv. Mater.*, 2013, **14**, 043502.

2 P. Knauth, *Solid State Ionics*, 2009, **180**, 911.

3 *Nanocomposites: Ionic Conducting Materials and Structural Spectroscopies*, ed. P. Knauth and J. Schoonman, Springer, Berlin, 2008.

4 A. Hayashi, K. Noi, A. Sakuda and M. Tatsumisago, *Nat. Commun.*, 2012, **3**, 856.

5 L. N. Patro and K. Hariharan, *Solid State Ionics*, 2013, **239**, 41.

6 J. Schoonman, K. Wapenaar, G. Oversluizen and G. Dirksen, *J. Electrochem. Soc.*, 1979, **126**, 709.

7 J. Schoonman and A. Wolfert, *J. Electrochem. Soc.*, 1981, **128**, 1522.

8 M. A. Reddy and M. Fichtner, *J. Mater. Chem.*, 2011, **21**, 17059.

9 C. Rongeat, M. A. Reddy, R. Witter and M. Fichtner, *J. Phys. Chem. C*, 2013, **117**, 4943.

10 I. Hanzu, A. Düvel, F. Preishuber-Pflügl, P. Heitjans and M. Wilkening, 2013, to be published.

11 V. Epp, z. Gün, H.-J. Deiseroth and M. Wilkening, *J. Phys. Chem. Lett.*, 2013, **4**, 2118.

12 A. Kuhn, S. Narayanan, L. Spencer, G. R. Goward, V. Thangadurai and M. Wilkening, *Phys. Rev. B: Condens. Matter Mater. Phys.*, 2011, **83**, 94302.

13 P. M. Richards, in *Topics in Current Physics*, ed. M. B. Salamon, Springer, Berlin, 1979, vol. 15.

14 P. Heitjans, A. Schirmer and S. Indris, in *Diffusion in Condensed Matter – Methods, Materials, Models*, ed. P. Heitjans and J. Kärger, Springer, Berlin, 2nd edn, 2005, ch. 9, pp. 369–415.

15 D. Brinkmann, *Prog. Nucl. Magn. Reson. Spectrosc.*, 1992, **24**, 527.

16 R. Böhmer, K. Jeffrey and M. Vogel, *Prog. Nucl. Magn. Reson. Spectrosc.*, 2007, **50**, 87.

17 M. Wilkening and P. Heitjans, *ChemPhysChem*, 2012, **13**, 53.

18 M. Wilkening and P. Heitjans, *Phys. Rev. B: Condens. Matter Mater. Phys.*, 2008, **77**, 024311.

19 H. Buschmann, J. Dölle, S. Berendts, A. Kuhn, P. Bottke, M. Wilkening, P. Heitjans, A. Senyshyn, H. Ehrenberg and A. Lotnyk, *et al.*, *Phys. Chem. Chem. Phys.*, 2011, **13**, 19378.

20 J. Langer, V. Epp, P. Heitjans, F. A. Mautner and M. Wilkening, *Phys. Rev. B: Condens. Matter Mater. Phys.*, 2013, **88**, 094304.

21 P. Heitjans and M. Wilkening, *Mater. Res. Bull.*, 2009, **34**, 915.

22 P. Heitjans, E. Tobschall and M. Wilkening, *Eur. Phys. J.: Spec. Top.*, 2008, **161**, 97.

23 A. Kuhn, M. Kunze, P. Sreeraj, H. D. Wiemhöfer, V. Thangadurai, M. Wilkening and P. Heitjans, *Solid State Nucl. Magn. Reson.*, 2012, **42**, 2.

24 A. Kuhn, P. Sreeraj, R. Pöttgen, H.-D. Wiemhöfer, M. Wilkening and P. Heitjans, *J. Am. Chem. Soc.*, 2011, **133**, 11018.

25 M. Wilkening, W. Küchler and P. Heitjans, *Phys. Rev. Lett.*, 2006, **97**, 065901.

26 M. Wilkening, V. Epp, A. Feldhoff and P. Heitjans, *J. Phys. Chem. C*, 2008, **112**, 9291.

27 K. Funke, *Prog. Solid State Chem.*, 1993, **22**, 111.

28 K. Funke, C. Cramer and D. Wilmer, in *Diffusion in Condensed Matter – Methods, Materials, Models*, ed. P. Heitjans and J. Kärger, Springer, Berlin, 2nd edn, 2005, ch. 21, pp. 857–893.

29 M. Meyer, P. Maass and A. Bunde, *Phys. Rev. Lett.*, 1993, **71**, 573.

30 A. Bunde, W. Dieterich, P. Maass and M. Meyer, in *Diffusion in Condensed Matter – Methods, Materials, Models*, ed. P. Heitjans and J. Kärger, Springer, Berlin, 2nd edn, 2005ch. 20, pp. 813–856.

31 D. R. Figueroa, A. V. Chadwick and J. H. Strange, *J. Phys. C: Solid State Phys.*, 1978, **11**, 55.

32 O. Kanert, R. Küchler, K. L. Ngai and H. Jain, *Phys. Rev. B: Condens. Matter Mater. Phys.*, 1994, **49**, 76.

33 K. Ngai, *Phys. Rev. B: Condens. Matter Mater. Phys.*, 1993, **48**, 13481.

34 V. Epp, O. Gün, H.-J. Deiseroth and M. Wilkening, *Phys. Chem. Chem. Phys.*, 2013, **15**, 7123.

35 K. L. Ngai, *Relaxation and Diffusion in Complex Systems*, Springer, New York, 2011.

36 D. L. Sidebottom, *Rev. Mod. Phys.*, 2009, **81**, 999.

37 J. R. Macdonald, *J. Appl. Phys.*, 1998, **84**, 812.

38 K. Ngai and C. León, *J. Non-Cryst. Solids*, 2003, **315**, 124.

39 D. Ailion and C. P. Slichter, *Phys. Rev. Lett.*, 1964, **12**, 168.

40 N. Bloembergen, E. M. Purcell and R. V. Pound, *Phys. Rev.*, 1948, **73**, 679.

41 V. Šepelák, A. Düvel, M. Wilkening, K.-D. Becker and P. Heitjans, *Chem. Soc. Rev.*, 2013, **42**, 7507.

42 B. Ruprecht, M. Wilkening, S. Steuernagel and P. Heitjans, *J. Mater. Chem.*, 2008, **18**, 5412.

43 B. Ruprecht, M. Wilkening, A. Feldhoff, S. Steuernagel and P. Heitjans, *Phys. Chem. Chem. Phys.*, 2009, **11**, 3071.

44 A. Düvel, B. Ruprecht, P. Heitjans and M. Wilkening, *J. Phys. Chem. C*, 2011, **115**, 23784.

45 A. Düvel, M. Wilkening, R. Uecker, S. Wegner, V. Šepelák and P. Heitjans, *Phys. Chem. Chem. Phys.*, 2010, **12**, 11251.

46 A. Düvel, S. Wegner, K. Efimov, A. Feldhoff, P. Heitjans and M. Wilkening, *J. Mater. Chem.*, 2011, **21**, 6238.

47 E. Fukushima and S. B. W. Roeder, *Experimental Pulse NMR: A Nuts and Bolts Approach*, Addison-Wesley Pub. Co., Advanced Book Program, Reading, Mass., 1981.

48 P. Heitjans, A. Schirmer and S. Indris, in *Diffusion in Condensed Matter*, ed. P. Heitjans and J. Kärger, Springer, 2005, ch. 9, p. 367.

49 C. P. Slichter and D. Ailion, *Phys. Rev.*, 1964, **135**, A1099.

50 D. C. Ailion and C. P. Slichter, *Phys. Rev.*, 1965, **137**, A235.

51 D. C. Look and I. J. Lowe, *J. Chem. Phys.*, 1966, **44**, 2995.

52 T. J. Rowland and F. Y. Fradin, *Phys. Rev.*, 1969, **182**, 760.

53 D. Wolf, *Phys. Rev. B: Solid State*, 1974, **10**, 2724.

54 K. E. D. Wapenaar, J. L. Van Koesveld and J. Schoonman, *Solid State Ionics*, 1981, **2**, 145.

55 A. K. Ivanov-Shits, N. I. Sorokin, P. P. Fedorov and B. P. Sobolev, *Solid State Ionics*, 1989, **31**, 269.

56 N. I. Sorokin and M. W. Breiter, *Solid State Ionics*, 1997, **99**, 241.

57 E. Barsis and A. Taylor, *J. Phys. Chem.*, 1968, **48**, 4357.

58 K. Funke and R. D. Banhatti, *J. Mater. Sci.*, 2007, **42**, 1942–1947.

59 B. Munro, M. Schrader and P. Heitjans, *Ber. Bunsenges. Phys. Chem.*, 1992, **96**, 1718.

60 H. Mehrer, *Diffusion in Solids*, Springer, Berlin, 2006.

61 F. Wang and C. P. Grey, *Chem. Mater.*, 1998, **10**, 3081.

62 J. Maier, *Prog. Solid State Chem.*, 1995, **23**, 171.

63 W. Puin, S. Rodewald, R. Ramlau, P. Heitjans and J. Maier, *Solid State Ionics*, 2000, **131**, 159.